Title

PET/MR Imaging of Malondialdehyde-Acetaldehyde Epitopes With a Human Antibody Detects Clinically Relevant Atherothrombosis.

Journal

Journal of the American College of Cardiology, 71(3)

ISSN

0735-1097

Authors

Senders, Max L
Que, Xuchu
Cho, Young Seok
et al.

Publication Date

2018

DOI

10.1016/j.jacc.2017.11.036

Peer reviewed

HHS Public Access

Author manuscript

J Am Coll Cardiol. Author manuscript; available in PMC 2018 June 11.

Published in final edited form as:

J Am Coll Cardiol. 2018 January 23; 71(3): 321–335. doi:10.1016/j.jacc.2017.11.036.

PET/MR Imaging of Malondialdehyde-Acetaldehyde Epitopes With a Human Antibody Detects Clinically Relevant Atherothrombosis

Max L. Senders, MD[a,b], **Xuchu Que, PhD**[c], **Young Seok Cho, MD, PhD**[d,e], **Calvin Yeang, MD, PhD**[e], **Hannah Groenen, BS**[a], **Francois Fay, PhD**[a,f], **Claudia Calcagno, MD, PhD**[a], **Anu E. Meerwaldt, MS**[a], **Simone Green, BS**[e], **Phuong Miu, BS**[e], **Mark E. Lobatto, MD, PhD**[g], **Thomas Reiner, PhD**[h,i], **Zahi A. Fayad, PhD**[a], **Joseph L. Witztum, MD**[c], **Willem J.M. Mulder, PhD**[a,b], **Carlos Pérez-Medina, PhD**[a], and **Sotirios Tsimikas, MD**[e]

[a]Translational and Molecular Imaging Institute, Icahn School of Medicine at Mount Sinai, New York, New York [b]Department of Medical Biochemistry, Academic Medical Center, Amsterdam, the Netherlands [c]Division of Endocrinology and Metabolism, Department of Medicine, University of California San Diego, La Jolla, California [d]Seoul National University College of Medicine, Seoul National University Bundang Hospital, Seoul, South Korea [e]Division of Cardiovascular Diseases, Sulpizio Cardiovascular Center, Department of Medicine, University of California San Diego, La Jolla, California [f]Department of Chemistry and Pharmaceutical Science, York College of The City University of New York, New York, New York [g]Department of Radiology, Academic Medical Center, Amsterdam, the Netherlands [h]Department of Radiology, Memorial Sloan Kettering Cancer Center, New York, New York [i]Department of Radiology, Weill Cornell Medical College, New York, New York

Abstract

BACKGROUND—Oxidation-specific epitopes (OSEs) are proinflammatory, and elevated levels in plasma predict cardiovascular events.

OBJECTIVES—The purpose of this study was to develop novel positron emission tomography (PET) probes to noninvasively image OSE-rich lesions.

METHODS—An antigen-binding fragment (Fab) antibody library was constructed from human fetal cord blood. After multiple rounds of screening against malondialdehyde-acetaldehyde (MAA) epitopes, the Fab LA25 containing minimal nontemplated insertions in the CDR3 region was identified and characterized. In mice, pharmacokinetics, biodistribution, and plaque specificity studies were performed with Zirconium-89 (^{89}Zr)-labeled LA25. In rabbits, ^{89}Zr-LA25 was used in combination with an integrated clinical PET/magnetic resonance (MR) system. ^{18}F-fluorodeoxyglucose PET and dynamic contrast-enhanced MR imaging were used to evaluate vessel wall inflammation and plaque neovascularization, respectively. Extensive ex vivo validation

ADDRESS FOR CORRESPONDENCE: Dr. Sotirios Tsimikas, Vascular Medicine Program, Department of Medicine, Sulpizio Cardiovascular Center, University of California San Diego, 9500 Gilman Drive, BSB 108, La Jolla, California 92093. stsimikas@ucsd.edu.; Dr. Carlos Pérez-Medina, Translational and Molecular Imaging Institute, Icahn School of Medicine at Mount Sinai, 1470 Madison Avenue, New York, New York 10029. carlos.perez-medina@mountsinai.org.

was carried out through a combination of gamma counting, near infrared fluorescence, autoradiography, immunohistochemistry, and immunofluorescence.

RESULTS—LA25 bound specifically to MAA epitopes in advanced and ruptured human atherosclerotic plaques with accompanying thrombi and in debris from distal protection devices. PET/MR imaging 24 h after injection of ^{89}Zr-LA25 showed increased uptake in the abdominal aorta of atherosclerotic rabbits compared with nonatherosclerotic control rabbits, confirmed by ex vivo gamma counting and autoradiography. ^{18}F-fluorodeoxyglucose PET, dynamic contrast-enhanced MR imaging, and near-infrared fluorescence signals were also significantly higher in atherosclerotic rabbit aortas compared with control aortas. Enhanced liver uptake was also noted in atherosclerotic animals, confirmed by the presence of MAA epitopes by immunostaining.

CONCLUSIONS—^{89}Zr-LA25 is a novel PET radiotracer that may allow noninvasive phenotyping of high-risk OSE-rich lesions.

Keywords

atherosclerosis; natural antibodies; oxidation-specific epitopes; PET/MR imaging

Atherosclerosis is a chronic, multifocal inflammatory disease of medium and large arteries and is the major underlying cause of cardiovascular disease (CVD). Despite a decline in mortality in the Western world, the prevalence of CVD has not decreased and remains the leading global cause of death (1). Progression of atherosclerosis is driven by the accumulation, modification, and oxidation of circulating lipids, which drives the influx of immune cells in the vessel wall, leading to chronic inflammation and the development of advanced atherosclerotic plaques. Progressing plaques are prone to develop erosion and/or rupture, resulting in the release of thrombotic material into the circulation that may lead to luminal occlusion and acute cardiovascular events (e.g., myocardial infarction and stroke) (2). A large subset of such plaques continues to grow until they cause myocardial ischemia, leading to angina pectoris. Moreover, an emerging paradigm focusing on superficial plaque erosion, departing from the classical thrombotic rupture has been suggested (3–5). Clinical practice relies on detecting ischemia of obstructive lesions to diagnose risk, leaving features like plaque burden and outward remodeling underappreciated (6). There is a need for accurate imaging methods to assess the extent of disease burden and to identify high-risk lesions, including those with superficial plaque erosion (7,8).

Oxidized low-density lipoprotein (OxLDL) and oxidized phospholipids (OxPL) have been identified as hallmarks of high cardiovascular risk (9–13). When low-density lipoprotein (LDL) undergoes oxidation, the byproducts of lipid peroxidation generate many proinflammatory chemical modifications of both the lipid and protein moieties, collectively termed oxidation-specific epitopes (OSEs). Several of these OSEs, such as OxPL and malondialdehyde (MDA) epitopes, are well defined chemically and immunologically. They represent danger-associated molecular patterns and induce a proinflammatory response (14,15). Additionally, prior work has shown that OSEs can be imaged in zebrafish, mice, and rabbit lipid/atherosclerosis models with murine or human OSE-targeted antibodies using nuclear and magnetic resonance (MR) imaging techniques (16–22). However, the potential immunogenicity of these approaches may limit clinical application (23,24).

Here, we report a multimodal positron emission tomography (PET)/MR evaluation using the human antibody Fab fragment LA25 binding to advanced MDA epitopes, namely malondialdehyde-acetaldehyde (MAA) adducts, which are OSEs found in human atherothrombotic lesions that may serve as a noninvasive imaging biomarker of atherosclerotic burden and plaque vulnerability.

METHODS

POSITRON EMISSION TOMOGRAPHY/MAGNETIC RESONANCE IMAGING

Rabbits (n = 12; mean weight: 3.4 ± 0.9 kg for rabbits with atherosclerosis, and 3.2 ± 0.1 kg for healthy control rabbits) (Online Figure 1). A 24-G catheter was introduced in the marginal ear vein for injection with either ^{89}Zr-LA25 or ^{89}Zr-LA24 (0.94 ± 0.22 mCi; 0.3 to 0.4 mg). In the contralateral ear, a 22-G catheter was used for the administration of the gadolinium-based contrast agent: gadopentetate dimeglumine (Magnevist, Bayer Healthcare, Shawnee Mission, Kansas, Missouri). Anesthesia was induced by intramuscular injection of Ketamine (20 mg/kg) (Fort Dodge Animal Health, Overland Park, Kansas, Missouri), together with Xylazine (0.5 mg/kg) (Bayer). Prior to ^{18}F-fluorodeoxyglucose (^{18}F-FDG) injections, rabbits were fasted for ≥4 h. All rabbits received a urine catheter to prevent any disruptions from signal in the bladder.

Rabbits were placed in a body matrix coil, received isoflurane anesthesia at 1.5% by inhalation, and were oxygenated for the remaining of the PET/MR imaging experiment while vital parameters were monitored. Shortly after injection, images were acquired in a dynamic fashion for 1 h using a clinical 3-T PET/MR Biograph mMR (Siemens, Munchen, Germany). After scout scans, the PET scan was initiated and coacquired with bright-blood time-of-flight (TOF) noncontrast enhanced angiography for localization of arterial anatomical landmarks (renal arteries and iliac bifurcation). Imaging parameters were: repetition time (TR), 23 ms; echo time (TE), 2.8 ms; flip angle, 20°; spatial resolution, 0.35 × 0.35 mm^2 (interpolated); slice thickness, 1 mm. Attenuation correction of PET images was done using the built-in MR-based attenuation correction map and segmenting it into 2 tissue compartments (soft tissue and air), and images reconstructed using the 3D ordinary Poisson ordered subsets expectation maximization (OP-OSEM) algorithm with point-spread-function (PSF) resolution modeling, using 3 iterations and 21 subsets. In addition, a black blood 3D T2 weighted SPACE (Sampling Perfection with Application optimized Contrasts using different flip angle Evolution) sequence was used for vessel wall delineation. Imaging parameters were: TR, 1600 ms; TE, 115 ms; flip angle, 120°; echo train length (ETL), 81; spatial resolution, 0.63 × 0.63 mm^2; slice thickness, 0.63 mm; fat saturation, on.

A dynamic contrast-enhanced (DCE) MR scan was performed. Black blood was obtained using a double inversion recovery technique. A 3-dimensional turbo-field echo sequence with motion-sensitized driven equilibrium preparation for black blood imaging was used to quantify the uptake of a Food and Drug Administration–approved gadolinium-based contrast agent (CA), gadopentetate dimeglumine (Magnevist), from the right renal artery to the iliac bifurcation. This protocol of black blood DCE-MR is explained in more detail by Calcagno et al. (25). Imaging parameters were: TR, 491 ms; TE, 5.3 ms; flip angle, 20°; spatial resolution, 0.63 × 0.63 mm^2; slice thickness, 0.63 mm; fat saturation, on; orientation,

sagittal. This sequence was used before and 10 min after CA injection to quantify the CA accumulation in the vessel wall and, thus, to measure the permeability of the vessel wall. Before and during CA injection, the same sequence was used with 3 signal averages (time resolution 32 s) to perform 3-dimensional DCE-MRI and to quantify the rate of uptake of CA in the vessel wall. The next day, 24 ± 1.5 h after injection, all rabbits received a 20-min static PET scan, again using a time-of-flight and MR-based attenuation correction.

PHARMACOKINETICS AND BIODISTRIBUTION OF ^{89}ZR-LA25 AND 89ZR-LA24 IN RABBITS

Radioactivity half-lives were determined by drawing blood from the ear arteries at 1 and 30 min; at 1, 2, 4, 20, and 24 h; and at sacrifice after 28 h. All rabbits were sacrificed by an intravenously injected overdose of 100 mg/kg sodium pentobarbital and were subsequently perfused with 500 ml saline. After sacrifice, all animals were perfused to make sure no blood or blood clots remained in the aorta and other organs before excision. Aortas were excised and divided into thoracic aorta (from the aortic root to the diaphragm) and abdominal aorta (from the diaphragm to the iliac bifurcation), the latter with celiac trunk and renal arteries attached, serving as landmarks. The following organs were harvested: heart, lungs, liver, spleen, kidneys, 1 adrenal gland, muscle, and bone marrow. All tissues were weighed before counting with a Wizard2 2480 (Perkin Elmer, Waltham, Massachusetts) automatic gamma counter. Radioactivity concentration in tissues was calculated as the percentage of injected dose (ID) per gram.

NEAR-INFRARED FLUORESCENCE IMAGING

At 24 h before sacrifice, all rabbits received fluorescently labeled (DiD) high-density lipoprotein (HDL) (~1 mg dye/rabbit) in 5-ml phosphate-buffered saline solution via the marginal ear vein. After sacrifice, all aortas, both thoracic and abdominal, were placed on thick black paper and imaged with a Xenogen IVIS-200 optical imaging system (Perkin Elmer, Waltham, Massachusetts). Fluorescence images were acquired with excitation and emission wavelengths of 680 and 720 nm and a field of view of 6.5 and 22.8 cm using different exposure times.

IMAGE ANALYSIS

Image analysis for PET imaging was performed after all data were processed and divided in different time frames using a custom-made program written in Matlab (Mathworks, Natick, Massachusetts). All data was subsequently processed using OsiriX Imaging Software (OsiriX Foundation, Geneva, Switzerland) by drawing regions of interest (ROIs) on the infrarenal abdominal aorta and major organs (liver, spleen, and kidneys). By averaging all acquired ROIs per organ (≥10 per organ), mean maximum standardized uptake values (SUVs) in each tissue were obtained. All images acquired with DCE-MR were reformatted in the axial plane for tracing. The vessel wall tracing was made on the average image of the dynamic series of DCE-MR using Osirix software (OsiriX Foundation, Geneva, Switzerland). By drawing an inner and an outer vessel wall contour and computing the difference between them, the vessel wall area or ROI was measured.

STATISTICAL ANALYSIS

Statistical analysis was conducted using nonparametric Mann-Whitney tests. Spearman's r coefficients were calculated to determine the degree of correlation. Data are reported as mean ± SD. All p values <0.05 were considered statistically significant. Prism software version 6.0 (GraphPad Software, La Jolla, California) was used to calculate the different statistical parameters.

The complete detailed methods section is provided in the Online Appendix.

RESULTS

CLONING AND CHARACTERIZATION OF LA25

LDL was modified with MAA, MDA, or $CuSO_4$ to generate MAA-LDL (Figure 1A) (26), MDA-LDL, and copper (Cu)-OxLDL, respectively. MAA is an advanced MDA-derived adduct that we and others have shown is an immunodominant MDA epitope (26–28). MAA is an adduct between a protein lysine residue, 2 MDAs, and 1 acetaldehyde molecule to generate a cyclic, fluorescent dihydropyridine product (such as the 4-methyl-1,4-dihydropyridine-3,5-dicarbonyl adduct) (Figure 1A). MAA is dissimilar to a simple linear MDA-lysine adduct and, therefore, would not be expected to be recognized by antibodies to MDA.

Lymphocytes were isolated from the umbilical cord blood of 7 newborns at birth, prior to any environmental exposure, to specifically enrich for germline sequences with minimal nontemplated insertions in the CDR3 region consistent with evolutionary conservation. κ and λ libraries containing 10^7–10^8 Fabs were then constructed, consisting of the LacZ promoter, the light chain, the heavy chain, and polyhistidine and hemagglutinin tags (Figure 1B). The libraries were screened against MAA-BSA, using methods previously described (29). After 4 rounds of panning with each κ and λ library, we identified an enrichment of Fabs that were cloned into the phagemid pComb3X. LA25 was identified as an optimal candidate due to its specificity for MAA epitopes and optimal expression characteristics. LA24, identified from the same library, did not bind any relevant OSE present in vivo and was subsequently used as a control in experiments. LA25 and LA24 plasmids from selected Fab phage clones were codon optimized and transformed into E. coli C41 (DE3) for production of soluble Fabs.

Binding and competition assays were then carried out to assess specificity for MAA epitopes. LA25 bound to MAA-LDL, but not to LDL, Cu-OxLDL or MDA-LDL (Figure 1C). LA24 did not detect any of these epitopes. To assess specificity of LA25 to bind to MAA epitopes, competition experiments were performed of LA25 binding to MAA-LDL (Figure 1D) and MAA-BSA (Figure 1E). These experiments demonstrated that a variety of MAA epitopes, in a hapten-specific manner, nearly completely inhibited the binding LA25 to its antigens. In contrast, MDA-BSA, MDA-LDL, Cu-OxLDL, and LDL did not compete for LA25 binding. To further assess in vivo specificity and also to gain insights into potential therapeutic applications of LA25, experiments were performed to assess whether LA25 inhibited binding of MAA-LDL to elicited peritoneal macrophages. Increasing doses of

LA25 almost completely inhibited binding of MAA-LDL to macrophages (Figure 1F), a property that is expected to be atheroprotective (15,26,29,30).

IMMUNOSTAINING OF HUMAN PATHOLOGIC SPECIMENS WITH LA25

Immunostaining of early human coronary lesions from patients with sudden death with LA25 showed minimal staining in pathological intimal thickening (PIT) samples, but significant staining in advanced fibroatheromas and ruptured plaques (Figure 2). Interestingly, LA25 also stained the thrombus adjacent to the plaque rupture. Thrombi are known to contain MDA/MAA epitopes, likely through secretion by activated platelets (31). Debris from distal protection devices also stained strongly with LA25, as well as for MDA and OxPL epitopes with specific antibodies (Figure 3). MAA epitopes did not colocalize with OxPL epitopes in these specimens, but MDA epitopes colocalized partially with both MAA and OxPL epitopes. LA24 did not stain coronary lesions or debris from distal protection devices.

PHARMACOKINETICS, BIODISTRIBUTION, AND PLAQUE SPECIFICITY OF ^{89}ZR-LA25 IN APOE$^{-/-}$ MICE

Initially, the ^{89}Zr-labeled Fabs (Online Figure 2A) were tested in *Apoe*$^{-/-}$mice to investigate their in vivo behavior and specificity for MAA epitopes in atherosclerotic plaques. Mice were intravenously injected with either ^{89}Zr-LA25 or -LA24 control Fab. The blood radioactivity half-lives were 29 and 13 min for LA25 and LA24, respectively, and blood radioactivity concentrations differed significantly starting at 30 min after injection (Figure 4A).

Radioactivity distribution in selected tissues was determined by gamma counting at 4 h post-injection (p.i.) (Online Figure 2B). Aortic uptake was significantly higher in mice injected with 89Zr-LA25 compared with ^{89}Zr-LA24 (1.56 ± 0.35% vs. 0.41 ± 0.13 %ID/g; p = 0.001) (Figure 4B). Representative autoradiography of mouse aortas showed homogenous radioactivity distribution in those injected with ^{89}Zr-LA24, whereas ^{89}Zr-LA25 showed a heterogeneous pattern of uptake with more intense depositions at the level of typical lesion sites, such as the aortic root and the abdominal aorta (arrows in Figure 4C).

A high kidney accumulation was found in all mice, which is indicative of renal clearance. Uptake in liver and spleen was significantly lower in mice injected with 89Zr-LA24 compared with 89Zr-LA25 (0.53 ± 0.12% vs. 3.50 ± 1.67 %ID/g; p = 0.001; and 0.63 ± 0.16% vs. 2.69 ± 1.03 %ID/g; p = 0.005, respectively) (Figure 4D).

Additionally, analysis by autoradiography and immunofluorescence of aortic root sections from mice injected with ^{89}Zr-LA25 revealed a high degree of colocalization between radioactivity and macrophages (CD68, red) (Figure 4E).

To investigate whether the difference in hepatic uptake was due to the presence of MAA, *Apoe*$^{-/-}$ mouse livers were stained with LA24 and LA25 (Figure 4F). While LA25 stained liver samples, no staining was observed in sections treated with LA24. This suggests that the presence of MAA may account for the difference in liver uptake between ^{89}Zr-LA25 and -

LA24, although the longer circulation half-life of 89Zr-LA25 may also contribute to a higher nonspecific binding.

PET/MR IMAGING IN RABBITS

Atherosclerotic rabbits were dynamically scanned for 1 h immediately after intravenous injection of either 89Zr-LA25 or -LA24 (Figure 5A), and statically at 24 h p.i. (timeline in Online Figure 3A). SUV were measured in kidney, liver, and spleen, showing an increase in kidney uptake and a slight decrease in liver and spleen uptake for both Fabs over the course of 24 h (Figure 5B). Liver uptake was significantly higher in rabbits injected with 89Zr-LA25 compared with ^{89}Zr-LA24. Concordant with mouse immunostaining results (Figure 4F), rabbit liver sections demonstrated specific staining with LA25 in areas of steatosis, with both intracellular and extracellular staining, whereas no staining was noted with LA24 (Online Figure 3B). Splenic uptake was also higher in rabbits injected with ^{89}Zr-LA25. Kidney uptake, however, was significantly higher for ^{89}Zr-LA24 during the first hour and 24 h post-injection. For an extensive biodistribution of the radiolabeled Fabs by PET in both healthy control and atherosclerotic rabbits, please see Online Figure 3C. Blood radioactivity half-life was longer for ^{89}Zr-LA25 than ^{89}Zr-LA24 (2.2 h vs. 1.1 h) (Figure 5C). Thus, as seen in mice (Figure 4A), the blood time-activity curve for ^{89}Zr-LA25 in rabbits also showed relatively delayed clearance, although clearance was fairly fast (<30 min) for both Fabs. Importantly, PET/MR quantification results were corroborated by ex vivo gamma counting. All rabbits were sacrificed at 28 h post-injection and tissues harvested after thorough perfusion. Radioactivity counting revealed a significantly higher aortic uptake for 89Zr-LA25 compared with 89Zr-LA24 in rabbits with atherosclerosis (0.022 ± 0.003% vs. 0.006 ± 0.001 %ID/g; $p = 0.02$) (Figure 5D).

Autoradiography corroborated earlier results in mice: a heterogeneous radioactivity distribution pattern was found in the ^{89}Zr-LA25 group in contrast with a homogenous distribution found for ^{89}Zr-LA24 (Figure 5E). Extended ex vivo biodistribution data are provided in Online Figure 4A.

PHENOTYPING OF RABBIT ATHEROSCLEROTIC PLAQUES

To noninvasively assess disease burden in healthy New Zealand White rabbits versus New Zealand White rabbits with atherosclerosis, we combined ^{89}Zr-LA25-PET with previously validated PET/MR imaging protocols. We simultaneously evaluated different hallmarks of advanced atherosclerotic plaques (i.e., OSEs, plaque area, and neo-vascularization), and assessed inflammation in an earlier session by ^{18}F-FDG-PET (Online Figure 3A).

^{89}Zr-LA25 uptake was evaluated in vivo by PET/MR 24 h after injection, when blood signal was low based on pharmacokinetic data (Online Figure 4B). Representative aortic coronal fused PET/MR images are shown in Figure 6A, in nonatherosclerotic and atherosclerotic rabbits injected with ^{89}Zr-LA25. Uptake in the vessel wall was quantified by drawing ROIs on the aorta from the left renal artery to the iliac bifurcation. Radioactivity uptake was higher for ^{89}Zr-LA25 in rabbits with atherosclerosis compared with healthy control rabbits, 0.33 ± 0.09 g/ml vs. 0.25 ± 0.05 g/ml (Figure 6A, right). The PET/MR findings were confirmed by autoradiography, showing a heterogeneous deposition pattern in

atherosclerotic aortas compared with the homogenous lower uptake found in control aortas (Figure 6B, left), and ex vivo gamma counting (28 h post-injection) revealed a significantly higher uptake for ^{89}Zr-LA25 in athero-sclerotic aortas (0.022 ± 0.003% vs. 0.005 ± 0.001 %ID/g; p = 0.02) (Figure 6B, right). Moreover, correlations between the target-to-blood ratio of aortas as determined by PET (as ratio to withdrawn blood) and gamma counting showed a significant positive correlation (r = 0.97; p < 0.0001) (Online Figure 4C).

A significantly larger vessel wall area was measured for rabbits with atherosclerosis compared with their healthy control counterparts (0.29 ± 0.06 mm^2 vs. 0.11 ± 0.03 mm^2; p = 0.03) (Figure 6C). At 48 h prior to ^{89}Zr-LA25 injection, inflammation was assessed by ^{18}F-FDG-PET. Uptake in the abdominal aorta was significantly higher in atherosclerotic rabbits compared with healthy control rabbits (1.95 ± 0.19 g/ml vs. 0.36 ± 0.02 g/ml; p = 0.02) (Figure 6D). DCE-MR imaging was used to evaluate vascular permeability, which was numerically higher in atherosclerotic rabbits compared with control rabbits (4.29 ± 1.61 vs. 1.82 ± 1.33; p = 0.11) (Figure 6E). We also used a fluorescently labeled reconstituted high-density lipoprotein (rHDL) nanoparticle as a macrophage mapping agent that was injected 24 h before sacrifice, as previously described (32). After euthanasia, all aortas were imaged by near infrared fluorescence (NIRF), which revealed approximately 100-fold higher fluorescence intensity in atherosclerotic aortas compared with control aortas (98 ± 16 × 10^9 vs. 1.14 ± 0.18 × 10^9 μW/cm^2; p = 0.03) (Figure 6F). In addition, NIRF imaging showed a heterogeneous fluorescence signal distribution in aortas from diseased rabbits, indicative of accumulation in atherosclerotic lesions.

Of note, we found a strong correlation between ^{89}Zr-LA25 radioactivity and rHDL NIRF intensity in aortas (r = 0.83; p = 0.02), possibly suggesting a certain degree of macrophage uptake of ^{89}Zr-LA25 (Online Figure 5). Strong correlations were found between rHDL fluorescence intensity and PET-derived FDG uptake (r = 0.67; p < 0.0001) (Online Figure 6A), and ex vivo–quantified ^{89}Zr-LA25 uptake and PET-derived FDG uptake (r = 0.79; p = 0.03) (Online Figure 6B). Moreover, a significant correlation between ^{89}Zr-LA25 radioactivity and plaque area was found by T2-weighted MR (r = 0.83; p = 0.02) (Online Figure 6C). However, uptake of ^{89}Zr-LA25 in the aorta showed no correlation with permeability as determined by DCE-MR (r = 0.57; p = 0.15) (Online Figure 6D).

Finally, to assess the feasibility of coronary imaging, we measured heart uptake by PET and calculated aorta-to-heart ratios for both ^{89}Zr-LA25 and ^{18}F-FDG. After a 4-h fast before injection, high myocardial uptake was observed for ^{18}F-FDG as expected, while radioactivity accumulation for ^{89}Zr-LA25 in the heart was low (Online Figure 7A). As a result, the aorta-to-heart ratio was 2.5-fold higher for 89Zr-LA25 compared with ^{18}F-FDG (0.96 ± 0.13 vs. 0.38 ± 0.19; p = 0.06) (Online Figure 7B). This favorable ratio was also measured ex vivo for 89Zr-LA25 (2.10 ± 0.23).

EX VIVO PLAQUE CHARACTERIZATION

After rabbits were sacrificed for ex vivo validation, 1 abdominal aorta was divided into several different pieces and processed for histology. The first section in a set of slides was used for autoradiography and adjacent sections were stained with hematoxylin and eosin: RAM-11 for macrophages and Oil Red O for lipid content; representative images are shown

in Figure 7. Significant positive correlations were found between ^{89}Zr-LA25 autoradiography integrated density (mean gray value) and vessel wall area in pixels ($r = 0.90$; $p < 0.0001$), macrophage area in pixels ($r = 0.72$; $p = 0.0008$), and lipid content ($r = 0.75$; $p = 0.0002$) (Figure 7).

DISCUSSION

This study demonstrates for the first time the noninvasive PET/MR imaging of proinflammatory MAA epitopes in the context of atherosclerosis in mice and rabbits using a radiolabeled human antibody fragment (Central Illustration). High and specific uptake in atherosclerotic lesions and liver tissue was demonstrated in 2 animal models of atherosclerosis. The evidence for detecting clinically relevant atherosclerotic lesions is reflected by the histological evaluation that showed intensely stained advanced human fibroatheromas, ruptured plaques and their accompanying thrombi, as well as debris from distal protection devices. Additionally, we observed enhanced hepatic uptake and immunohistological evidence of MAA epitopes in the liver, suggesting that this may be a viable imaging biomarker to assess OSE accumulation in liver diseases.

Initial nuclear in vivo imaging studies targeting OSEs using the murine radiolabeled monoclonal antibody MDA2 showed specific uptake in mouse and rabbit atherosclerotic aortas (17,33,34). More recently, gadolinium (18), manganese (21), and ultrasmall superparamagnetic iron oxide (20) nanoparticles decorated with 3 different OSE-targeted antibodies or antibody fragments confirmed their utility as MR imaging contrast agents in mice. However, despite the proven feasibility of these imaging approaches as proof-of-concept in targeting OSE, potential toxicity of paramagnetic metals (35), long circulation times, relative lack of sensitivity, and potential immunogenicity of such antibodies are major obstacles for clinical translation. In contrast, LA25 represents a human Fab antibody that was derived from newborns with minimal nontemplated insertions in the CDR3 region typical of natural antibodies. It therefore represents a class of antibodies that will be theoretically safer to translate clinically because they are fully human, require no structural manipulation for human use, and are also evolutionarily selected to have putative beneficial functions, such as clearing apoptotic cells containing OSEs or protecting against bacterial infections (15). In addition, the small size of the LA25 Fab fragment facilitates rapid renal excretion, resulting in short circulating half-lives and allowing optimal plaque-to-blood ratios for noninvasive imaging.

Interestingly, blood circulating times were longer for ^{89}Zr-LA25 compared with ^{89}Zr-LA24 in atherosclerotic mice and rabbits, an observation consistent with prior studies using similar radiolabeled and OSE-targeted antibodies in nanoparticle formulations (17,18,20,21). The presence of circulating carriers of OSEs has been reported in the past, not only on circulating oxidized lipoproteins (34,36), but also on dying cells and microvesicles (37,38). All of these circulating MAA-bearing species serve as potential binding targets for ^{89}Zr-LA25 and may thus extend its half-life compared with ^{89}Zr-LA24. However, a limitation of this study is that the mechanism for this difference was not fully elucidated and needs to be evaluated in future investigations.

Increased uptake in the liver was also noted with ^{89}Zr-LA25, along with immunohistological evidence of the presence of MAA epitopes. Indeed, MAA and oxidized phospholipid epitopes are enriched in nonalcoholic fatty liver disease and both alcoholic and nonalcoholic steatohepatitis (39–42). In that regard, the high and specific liver uptake of ^{89}Zr-LA25 may also allow imaging of the presence of OSEs in humans with these conditions. With a global prevalence of liver steatosis around 25%, future research to further exploit the diagnostic capabilities of LA25-based radiotracers as imaging tools to noninvasively appraise fatty liver diseases might be warranted.

PET imaging showed increased radioactivity uptake for ^{89}Zr-LA25 in atherosclerotic aortas compared with both healthy control aortas and to the control antibody LA24 in atherosclerotic aortas. In addition, fluorescent rHDL and ^{89}Zr-LA25 showed similar distribution patterns in atherosclerotic aortas, as established by NIRF imaging and autoradiography. These findings suggest preferential accumulation of ^{89}Zr-LA25 in atherosclerotic lesions throughout the aorta. Strong correlations between ^{89}Zr-LA25 radioactivity uptake measured by gamma counting and previously validated imaging methods to measure atherosclerosis burden were found, further substantiating the notion of a specific accumulation in atherosclerotic lesions. As both ^{18}F-FDG and rHDL serve as markers for macrophage accumulation and activity, the strong observed correlations suggest a high degree of colocalization of 89Zr-LA25 with macrophages, as observed in mice by immunofluorescence. Because OxLDL with concomitant OSEs is engulfed by macrophages, these findings further strengthen our hypothesis that ^{89}Zr-LA25-bound OxLDL is taken up by macrophages in atherosclerotic lesions. Macrophages undergoing apoptosis and/or necrosis, as well as microvesicles, which bear OSEs, would also similarly bind LA25 and may account for the strong LA25 staining of necrotic areas noted in the human tissues.

Through development of different tracers and contrast agents targeting different hallmarks of plaque progression, molecular imaging has provided new insight into the pathophysiology of atherosclerosis (7,43). As a result, plaque inflammation has been widely studied in several animal models as well as in humans using 18F-FDG (44), and hypoxia-induced neovascularization in the plaque has been imaged by DCE-MR imaging (45). Moreover, recent studies have reported the use of radiotracers to evaluate a variety of processes involved in plaque progression, such as microcalcification (46), angiogenesis (47), and macrophage proliferation (48). Indeed, 89Zr-LA25 shows promise as a coronary atherosclerosis PET imaging agent given its ~2.5-fold higher aorta/myocardial uptake ratio in diseased animals than the currently approved 18F-FDG. Although this would potentially allow for better identification of lesions in these arteries, further optimization is needed because both the absolute uptake and the ratio itself were low at the selected imaging time point.

In a quest to predict future events, imaging studies have primarily focused on these well-known characteristics in individual plaques. However, focusing on culprit lesions has resulted in poor predictive value, and recent insights suggest that our attention should rather be on the total atherosclerotic disease burden (3). In this setting, radiotracers might be attractive candidates to assess the degree and extent of atherosclerosis as a systemic disease and eventually monitor therapeutic response. Recent data from the SPARCL (Lipitor in the

Prevention of Stroke, for Patients Who Have Had a Previous Stroke) trial show that apolipoprotein B-100–bound oxidized phospholipids are an excellent predictor of recurrent stroke and first major coronary events in patients with prior stroke or transient ischemic attack, despite treatment with high-dose atorvastatin (13). Therefore, OSE-targeted radio-labeled LA25 may aid disease management in patients who are at high risk of developing cardiovascular events (e.g., best medical treatment vs. preventive interventions, as in [a]symptomatic carotid disease). Moreover, to prove statistical differences, randomized controlled trials often require large subsets of patients that need to be followed up until reaching endpoints, typically mortality; this leads to a long and costly process. In this setting, imaging can assist in the development of new cardiovascular therapies by evaluating atherosclerosis burden, serving as a reliable readout in the assessment of treatment response (49).

STUDY LIMITATIONS

In this study, LA25 was labeled with the long-lived ^{89}Zr to facilitate extensive ex vivo characterization. For clinical application, the use of a shorter-lived radioisotope whose physical half-life matches the biological half-life of the Fab such as ^{64}Cu is preferable. In addition, and based on pharmacokinetic data, imaging at an earlier time after injection of the radiotracer would be desirable. Partial volume effects might have influenced the values in the aortic vessel wall, although maximum SUV is a well-established parameter in nuclear imaging (50). In a clinical scenario, however, target-to-blood ratios could compensate for these effects, which is not possible in rabbits. Although currently limited to research purposes, PET/MR imaging use for evaluating atherosclerosis is superior to PET/CT without compromising accuracy as we have shown with a significant positive correlation between ex vivo and in vivo uptake of ^{89}Zr-LA25 in rabbit aortas, and previously for other agents (32,51).

CONCLUSIONS

LA25 detects MAA epitopes, immunostains advanced human atherosclerotic lesions and may facilitate noninvasive imaging of atherosclerosis using PET imaging. This radiotracer could further help characterize the disease process and ultimately serve as a marker in a clinical setting to evaluate and inform therapeutic interventions.

Supplementary Material

Refer to Web version on PubMed Central for supplementary material.

Acknowledgments

This work was supported by Fondation Leducq grants R01-HL119828, R01-HL078610, R01-HL106579, R01 HL128550, R01 HL136098, P01 HL136275, R35 HL135737, and P01-HL055798 (to Dr. Tsimikas and/or Dr. Witztum), NIH-PPG grant HL 088093 (to Dr. Witztum), R01 EB009638 (to Dr. Fayad), and P01-HL131478 and R01-HL125703 (to Dr. Mulder); and by American Heart Association grant 16SDG31390007 (to Dr. Pérez-Medina). Dr. Senders is supported by American Heart Association grant 17PRE33660729 and the Foundation “De Drie Lichten” in the Netherlands. Drs. Que, Witztum, and Tsimikas are coinventors and receive royalties from patents owned by the University of California San Diego on oxidation-specific antibodies. Dr. Witztum has served as a consultant to Ionis Pharmaceuticals. Dr. Tsimikas has a dual appointment at the University of California San Diego and Ionis Pharmaceuticals. All other authors have reported that they have no relationships relevant to the contents of

this paper to disclose. Drs. Senders and Que contributed equally to this work and are joint first authors. Drs. Witztum, Perez-Medina, and Tsimikas contributed equally to this work and are senior authors. Jan Nilsson, MD, served as Guest Editor for this paper.

APPENDIX

For supplemental methods and figures, please see the online version of this paper.

ABBREVIATIONS AND ACRONYMS

DCE	dynamic contrast enhanced
Fab	antigen-binding fragment
ID	injected dose
MAA	malondialdehyde-acetaldehyde
MR	magnetic resonance
NIRF	near infrared fluorescence
OSE	oxidation-specific epitope
OxLDL	oxidized low-density lipoprotein
PET	positron emission tomography
SUV	standardized uptake value

References

1. Mozaffarian D, Benjamin EJ, Go AS, et al. Heart disease and stroke statistics–2016 update: A report from the American Heart Association. Circulation. 2016; 133:e38–360. [PubMed: 26673558]
2. Otsuka F, Kramer MC, Woudstra P, et al. Natural progression of atherosclerosis from pathologic intimal thickening to late fibroatheroma in human coronary arteries: a pathology study. Atherosclerosis. 2015; 241:772–82. [PubMed: 26058741]
3. Arbab-Zadeh A, Fuster V. The myth of the “vulnerable plaque”: transitioning from a focus on individual lesions to atherosclerotic disease burden for coronary artery disease risk assessment. J Am Coll Cardiol. 2015; 65:846–55. [PubMed: 25601032]
4. Libby P, Pasterkamp G. Requiem for the ‘vulnerable plaque’. Eur Heart J. 2015; 36:2984–7. [PubMed: 26206212]
5. Franck G, Mawson T, Sausen G, et al. Flow perturbation mediates neutrophil recruitment and potentiates endothelial injury via TLR2 in mice: implications for superficial erosion. Circ Res. 2017; 121:31–42. [PubMed: 28428204]
6. Varnava AM, Mills PG, Davies MJ. Relationship between coronary artery remodeling and plaque vulnerability. Circulation. 2002; 105:939–43. [PubMed: 11864922]
7. Dweck MR, Aikawa E, Newby DE, et al. Noninvasive molecular imaging of disease activity in atherosclerosis. Circ Res. 2016; 119:330–40. [PubMed: 27390335]
8. Higuma T, Soeda T, Abe N, et al. A Combined optical coherence tomography and intravascular ultrasound study on plaque rupture, plaque erosion, and calcified nodule in patients with ST-segment elevation myocardial infarction: incidence, morphologic characteristics, and outcomes after percutaneous coronary intervention. J Am Coll Cardiol Intv. 2015; 8:1166–76.

9. Tsimikas S, Willeit P, Willeit J, et al. Oxidation-specific biomarkers, prospective 15-year cardiovascular and stroke outcomes, and net reclassification of cardiovascular events. J Am Coll Cardiol. 2012; 60:2218–29. [PubMed: 23122790]
10. Tsimikas S, Duff GW, Berger PB, et al. Pro-inflammatory interleukin-1 genotypes potentiate the risk of coronary artery disease and cardiovascular events mediated by oxidized phospholipids and lipoprotein(a). J Am Coll Cardiol. 2014; 63:1724–34. [PubMed: 24530664]
11. Byun YS, Lee JH, Arsenault BJ, et al. Relationship of oxidized phospholipids on apolipoprotein B-100 to cardiovascular outcomes in patients treated with intensive versus moderate atorvastatin therapy: the TNT trial. J Am Coll Cardiol. 2015; 65:1286–95. [PubMed: 25835440]
12. van der Valk FM, Bekkering S, Kroon J, et al. Oxidized phospholipids on lipoprotein(a) elicit arterial wall inflammation and an inflammatory monocyte response in humans. Circulation. 2016; 134:611–24. [PubMed: 27496857]
13. Byun YS, Yang X, Bao W, et al. Oxidized phospholipids on apolipoprotein B-100 and recurrent ischemic events following stroke or transient ischemic attack. J Am Coll Cardiol. 2017; 69:147–58. [PubMed: 28081824]
14. Miller YI, Choi SH, Wiesner P, et al. Oxidation-specific epitopes are danger-associated molecular patterns recognized by pattern recognition receptors of innate immunity. Circ Res. 2011; 108:235–48. [PubMed: 21252151]
15. Binder CJ, Papac-Milicevic N, Witztum JL. Innate sensing of oxidation-specific epitopes in health and disease. Nat Rev Immunol. 2016; 16:485–97. [PubMed: 27346802]
16. Fang L, Green SR, Baek JS, et al. In vivo visualization and attenuation of oxidized lipid accumulation in hypercholesterolemic zebrafish. J Clin Invest. 2011; 121:4861–9. [PubMed: 22105168]
17. Tsimikas S, Palinski W, Halpern SE, Yeung DW, Curtiss LK, Witztum JL. Radiolabeled MDA2, an oxidation-specific, monoclonal antibody, identifies native atherosclerotic lesions in vivo. J Nucl Cardiol. 1999; 6:41–53. [PubMed: 10070840]
18. Briley-Saebo KC, Shaw PX, Mulder WJ, et al. Targeted molecular probes for imaging atherosclerotic lesions with magnetic resonance using antibodies that recognize oxidation-specific epitopes. Circulation. 2008; 117:3206–15. [PubMed: 18541740]
19. Li D, Patel AR, Klibanov AL, et al. Molecular imaging of atherosclerotic plaques targeted to oxidized LDL receptor LOX-1 by SPECT/CT and magnetic resonance. Circ Cardiovasc Imaging. 2010; 3:464–72. [PubMed: 20442371]
20. Briley-Saebo KC, Cho YS, Shaw PX, et al. Targeted iron oxide particles for in vivo magnetic resonance detection of atherosclerotic lesions with antibodies directed to oxidation-specific epitopes. J Am Coll Cardiol. 2011; 57:337–47. [PubMed: 21106318]
21. Briley-Saebo KC, Nguyen TH, Saeboe AM, et al. In vivo detection of oxidation-specific epitopes in atherosclerotic lesions using biocompatible manganese molecular magnetic imaging probes. J Am Coll Cardiol. 2012; 59:616–26. [PubMed: 22300697]
22. Khamis RY, Woollard KJ, Hyde GD, et al. Near infrared fluorescence (NIRF) molecular imaging of oxidized LDL with an autoantibody in experimental atherosclerosis. Sci Rep. 2016; 6:21785. [PubMed: 26911995]
23. Chou MY, Fogelstrand L, Hartvigsen K, et al. Oxidation-specific epitopes are dominant targets of innate natural antibodies in mice and humans. J Clin Invest. 2009; 119:1335–49. [PubMed: 19363291]
24. Tsiantoulas D, Sage AP, Mallat Z, Binder CJ. Targeting B cells in atherosclerosis: closing the gap from bench to bedside. Arterioscler Thromb Vasc Biol. 2015; 35:296–302. [PubMed: 25359862]
25. Calcagno C, Lobatto ME, Dyvorne H, et al. Three-dimensional dynamic contrast-enhanced MRI for the accurate, extensive quantification of microvascular permeability in atherosclerotic plaques. NMR Biomed. 2015; 28:1304–14. [PubMed: 26332103]
26. Duryee MJ, Klassen LW, Schaffert CS, et al. Malondialdehyde-acetaldehyde adduct is the dominant epitope after MDA modification of proteins in atherosclerosis. Free Radic Biol Med. 2010; 49:1480–6. [PubMed: 20696236]
27. Weismann D, Hartvigsen K, Lauer N, et al. Complement factor H binds malondialdehyde epitopes and protects from oxidative stress. Nature. 2011; 478:76–81. [PubMed: 21979047]

28. Gonen A, Hansen LF, Turner WW, et al. Atheroprotective immunization with malondialdehyde-modified LDL is hapten specific and dependent on advanced MDA adducts: implications for development of an atheroprotective vaccine. J Lipid Res. 2014; 55:2137–55. [PubMed: 25143462]
29. Shaw PX, Horkko S, Tsimikas S, et al. Human-derived anti-oxidized LDL autoantibody blocks uptake of oxidized LDL by macrophages and localizes to atherosclerotic lesions in vivo. Arterioscler Thromb Vasc Biol. 2001; 21:1333–9. [PubMed: 11498462]
30. Tsimikas S, Miyanohara A, Hartvigsen K, et al. Human oxidation-specific antibodies reduce foam cell formation and atherosclerosis progression. J Am Coll Cardiol. 2011; 58:1715–27. [PubMed: 21982317]
31. Fogelman AM, Shechter I, Seager J, Hokom M, Child JS, Edwards PA. Malondialdehyde alteration of low density lipoproteins leads to cholesteryl ester accumulation in human monocyte-macrophages. Proc Natl Acad Sci U S A. 1980; 77:2214–8. [PubMed: 6769124]
32. Perez-Medina C, Binderup T, Lobatto ME, et al. In vivo PET imaging of HDL in multiple atherosclerosis models. J Am Coll Cardiol Img. 2016; 9:950–61.
33. Tsimikas S, Shortal BP, Witztum JL, Palinski W. In vivo uptake of radiolabeled MDA2, an oxidation-specific monoclonal antibody, provides an accurate measure of atherosclerotic lesions rich in oxidized LDL and is highly sensitive to their regression. Arterioscler Thromb Vasc Biol. 2000; 20:689–97. [PubMed: 10712392]
34. Torzewski M, Shaw PX, Han KR, et al. Reduced in vivo aortic uptake of radiolabeled oxidation-specific antibodies reflects changes in plaque composition consistent with plaque stabilization. Arterioscler Thromb Vasc Biol. 2004; 24:2307–12. [PubMed: 15528482]
35. Sadowski EA, Bennett LK, Chan MR, et al. Nephrogenic systemic fibrosis: risk factors and incidence estimation. Radiology. 2007; 243:148–57. [PubMed: 17267695]
36. Tsimikas S, Palinski W, Witztum JL. Circulating autoantibodies to oxidized LDL correlate with arterial accumulation and depletion of oxidized LDL in LDL receptor-deficient mice. Arterioscler Thromb Vasc Biol. 2001; 21:95–100. [PubMed: 11145939]
37. Tsiantoulas D, Perkmann T, Afonyushkin T, et al. Circulating microparticles carry oxidation-specific epitopes and are recognized by natural IgM antibodies. J Lipid Res. 2014; 56:440–8. [PubMed: 25525116]
38. Chang MK, Bergmark C, Laurila A, et al. Monoclonal antibodies against oxidized low-density lipoprotein bind to apoptotic cells and inhibit their phagocytosis by elicited macrophages: evidence that oxidation-specific epitopes mediate macrophage recognition. Proc Natl Acad Sci U S A. 1999; 96:6353–8. [PubMed: 10339591]
39. Ikura Y, Ohsawa M, Suekane T, et al. Localization of oxidized phosphatidylcholine in nonalcoholic fatty liver disease: impact on disease progression. Hepatology. 2006; 43:506–14. [PubMed: 16496325]
40. Kwon HJ, Won YS, Park O, et al. Aldehyde dehydrogenase 2 deficiency ameliorates alcoholic fatty liver but worsens liver inflammation and fibrosis in mice. Hepatology. 2014; 60:146–57. [PubMed: 24492981]
41. Bieghs V, Walenbergh SM, Hendrikx T, et al. Trapping of oxidized LDL in lysosomes of Kupffer cells is a trigger for hepatic inflammation. Liver Int. 2013; 33:1056–61. [PubMed: 23617943]
42. Busch CJ, Hendrikx T, Weismann D, et al. Malondialdehyde epitopes are sterile mediators of hepatic inflammation in hypercholesterolemic mice. Hepatology. 2017; 65:1181–95. [PubMed: 27981604]
43. Mulder WJ, Jaffer FA, Fayad ZA, Nahrendorf M. Imaging and nanomedicine in inflammatory atherosclerosis. Sci Transl Med. 2014; 6:239sr1. [PubMed: 24898749]
44. Tawakol A, Migrino RQ, Bashian GG, et al. In vivo 18F-fluorodeoxyglucose positron emission tomography imaging provides a noninvasive measure of carotid plaque inflammation in patients. J Am Coll Cardiol. 2006; 48:1818–24. [PubMed: 17084256]
45. Calcagno C, Mani V, Ramachandran S, Fayad ZA. Dynamic contrast enhanced (DCE) magnetic resonance imaging (MRI) of atherosclerotic plaque angiogenesis. Angiogenesis. 2010; 13:87–99. [PubMed: 20526859]

46. Joshi NV, Vesey AT, Williams MC, et al. 18F-fluoride positron emission tomography for identification of ruptured and high-risk coronary atherosclerotic plaques: a prospective clinical trial. Lancet. 2014; 383:705–13. [PubMed: 24224999]

47. Beer AJ, Pelisek J, Heider P, et al. PET/CT imaging of integrin alphavbeta3 expression in human carotid atherosclerosis. J Am Coll Cardiol Img. 2014; 7:178–87.

48. Ye YX, Calcagno C, Binderup T, et al. Imaging macrophage and hematopoietic progenitor proliferation in atherosclerosis. Circ Res. 2015; 117:835–45. [PubMed: 26394773]

49. Fayad ZA, Mani V, Woodward M, et al. Safety and efficacy of dalcetrapib on atherosclerotic disease using novel non-invasive multimodality imaging (dal-PLAQUE): a randomised clinical trial. Lancet. 2011; 378:1547–59. [PubMed: 21908036]

50. Chen W, Dilsizian V. PET assessment of vascular inflammation and atherosclerotic plaques: SUV or TBR? J Nucl Med. 2015; 56:503–4. [PubMed: 25722451]

51. Robson PM, Dweck MR, Trivieri MG, et al. Coronary artery PET/MR imaging: feasibility, limitations, and solutions. J Am Coll Cardiol Img. 2017; 10(Pt A):1103–12.

PERSPECTIVES

COMPETENCY IN MEDICAL KNOWLEDGE

Proinflammatory, oxidation-specific epitopes are present in atherosclerotic lesions and steatotic livers, and elevated plasma levels predict cardiovascular events. Radiolabeled human antibody fragments such as ^{89}Zr-LA25 allow PET imaging of these epitopes.

TRANSLATIONAL OUTLOOK

Further research with ^{89}Zr-LA25–based imaging could facilitate disease localization and risk prediction and guide therapeutic interventions.

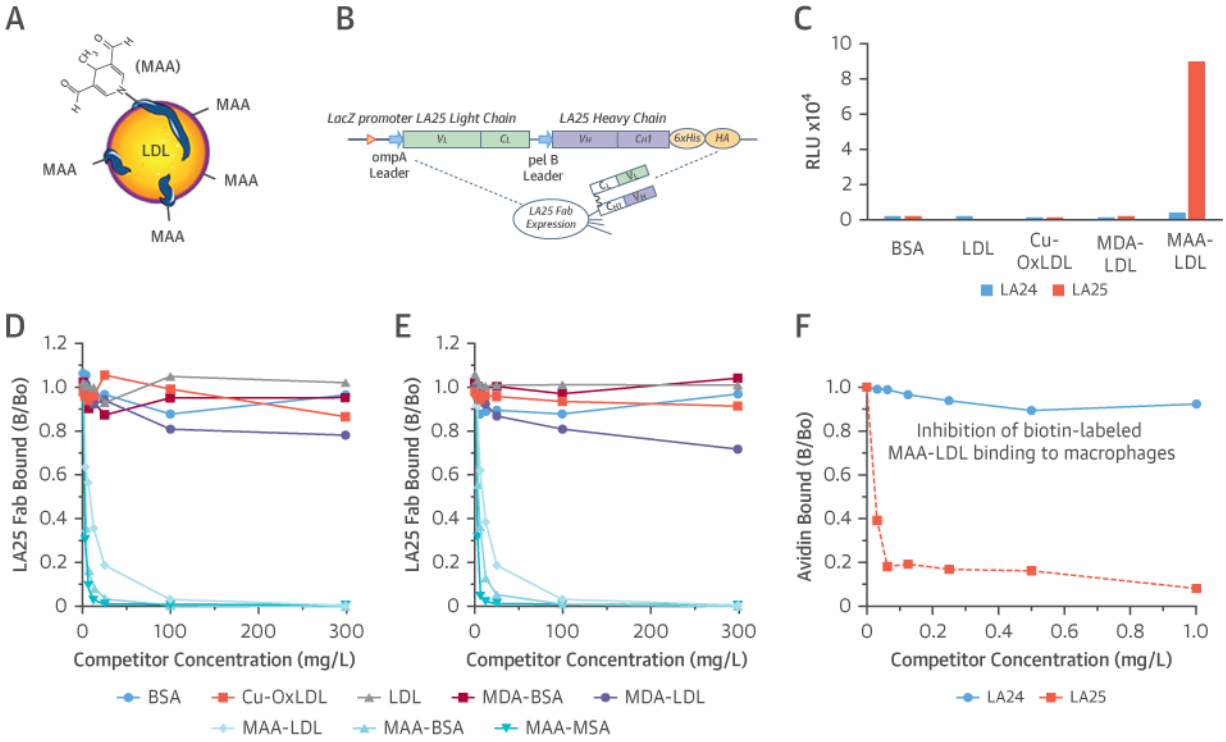

FIGURE 1. Cloning and Characterization of the MAA-Targeted LA25 Antibody Fragment

(A) Schematic depiction of malondialdehyde-acetaldehyde (MAA) low-density lipoprotein (LDL). **(B)** The configuration of soluble LA25 Fab antibody fragment. The LA25 lambda light-chain and heavy-chain with a hexa-histidine and the influenza hemagglutinin (HA) epitope tag for detection and purification were expressed under the direction of lacZ promoter for phage display or Fab production in E. coli. Proteolysis of the ompA and pelB signal peptides in the periplasm generated the native amino terminus of Fab and facilitated the joining of heavy and light chains together by disulfide bonds as bioactive soluble Fab. **(C)** Binding of LA25 to a variety of oxidation-specific epitopes. Competition assays for the specificity of LA25 binding to MAA-LDL **(D)** and MAA-BSA **(E)**. LA25 was incubated in the absence and presence of increasing amounts of indicated competitors, and the extent of binding to plated MAA-BSA and MAA-LDL was determined. Inhibition of MAA-LDL binding to macrophage scavenger receptors by LA25 **(F)**. Data are expressed as a ratio of binding in the presence of competitor (B) divided by absence of competitor (B_0). BSA = bovine serum albumin; Cu-OxLDL = copper-oxidized low-density lipoprotein; MDA = malondialdehyde; MSA = mouse serum albumin.

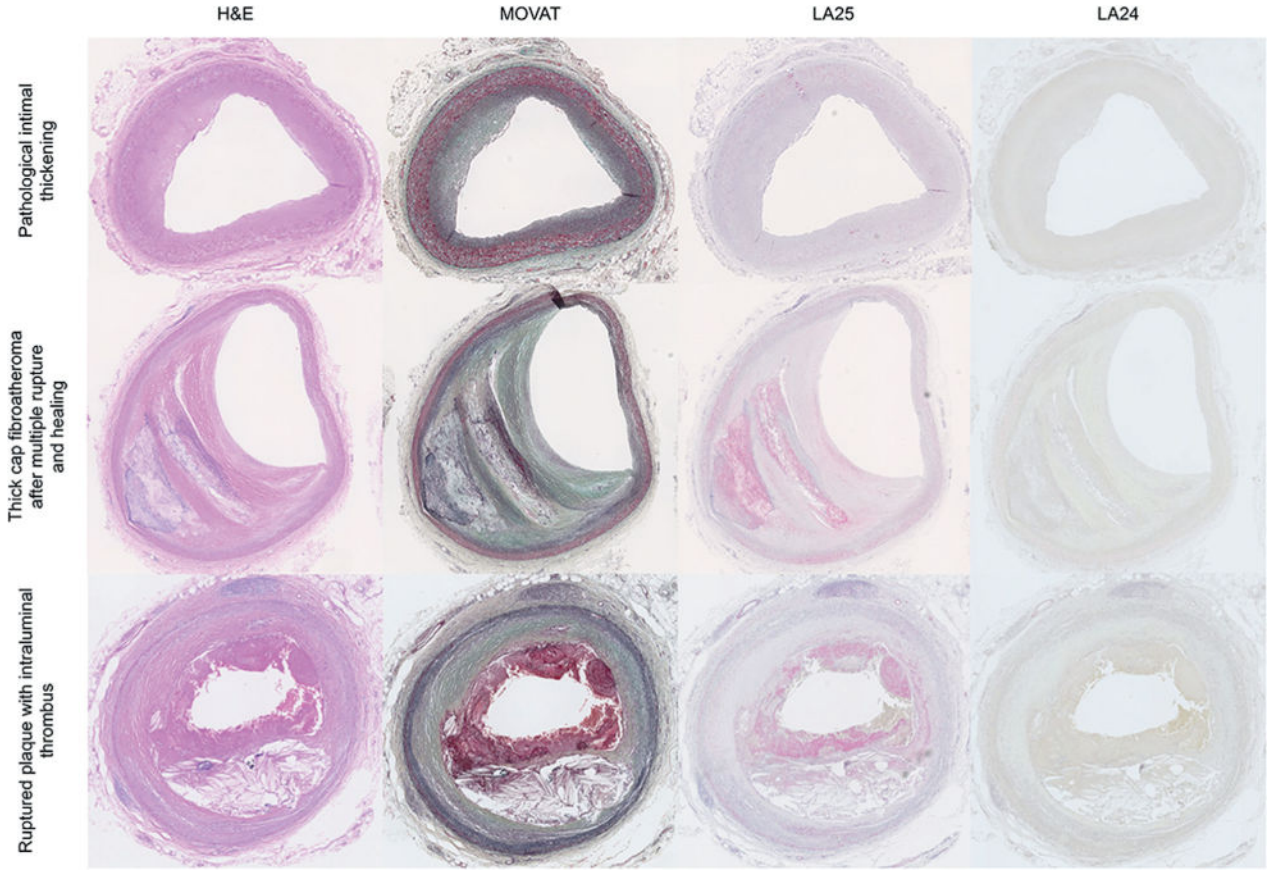

FIGURE 2. Immunostaining of Human Pathological Specimens With LA25

Immunostaining with LA25 and control antibody LA24 of coronary artery specimens representing pathological intimal thickening **(top row)**, thick cap fibroatheroma with multiple ruptures and healing phases **(middle row)** and a ruptured plaque containing thrombus **(bottom row)**, stained with hematoxylin and eosin (H&E), Movat pentachrome, LA25, and LA24 Fab control. Note the presence of thrombus in this section, which also stains with LA25.

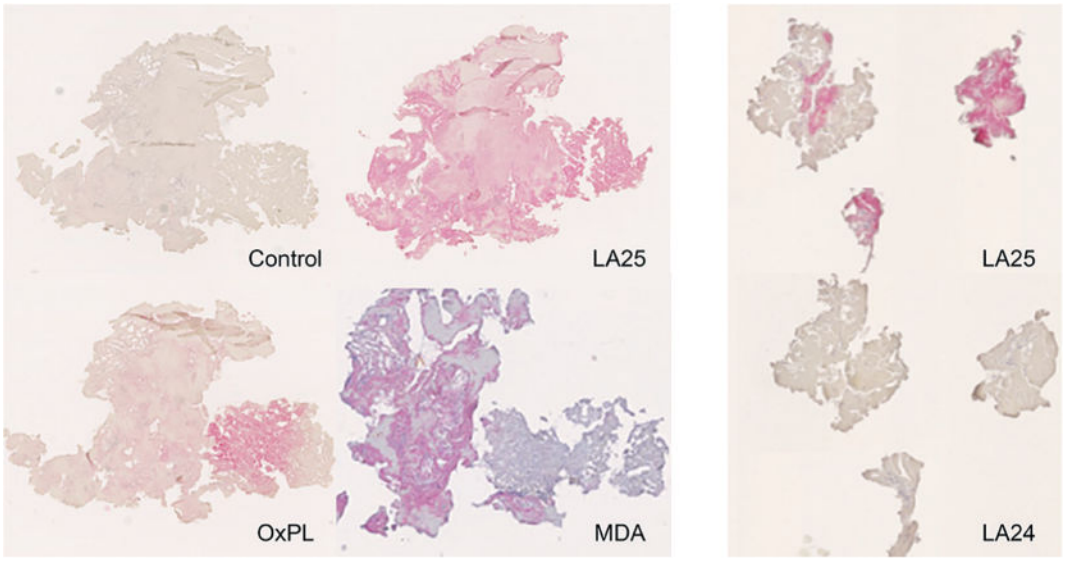

FIGURE 3. Immunostaining of Sections From Embolized Plaque Debris With LA25

Captured plaque debris from 2 distal protection devices following percutaneous coronary intervention. The material was stained with LA25 for malondialdehyde-acetaldehyde (MAA) epitopes, MDA3 antibody for MDA epitopes, and E06 antibody for OxPL epitopes. No-antibody (control) and LA24 control sections are also shown. MDA = malondialdehyde; OxPL = Oxidized phospholipids.

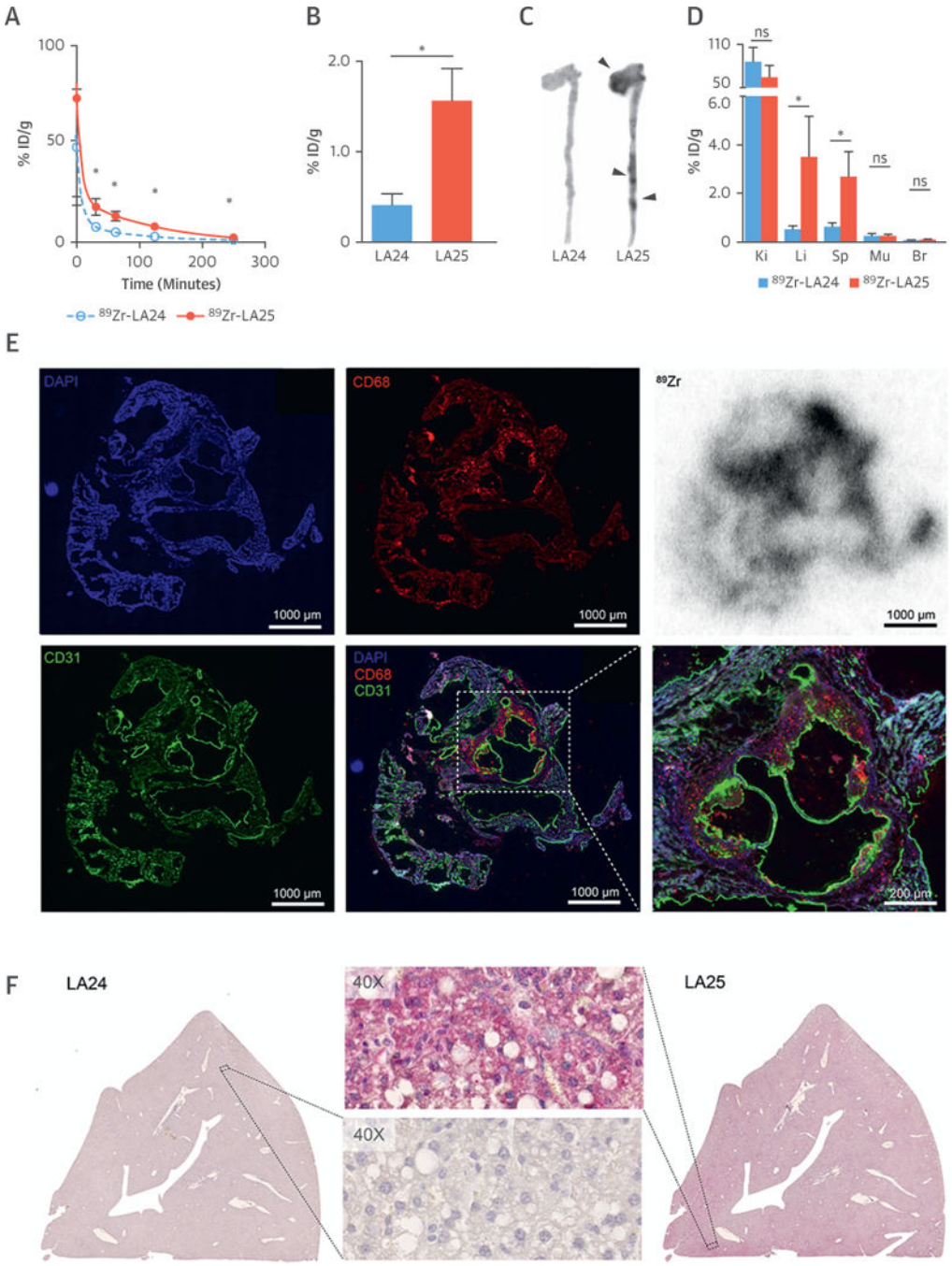

FIGURE 4. ^{89}Zr-LA25 Evaluation in *Apoe*$^{-/-}$ Mice

(A) Blood time-activity curve for ^{89}Zr-LA25 and -LA24. Gamma counting **(B)** and autoradiography **(C)** of aortas from *Apoe*$^{-/-}$ mice injected with ^{89}Zr-LA24 **(blue)** and ^{89}Zr-LA25 **(red)**. **(D)** Radioactivity distribution in selected tissues in *Apoe*$^{-/-}$ mice 4 h post-injection. **(E)** From **left to right, top row**: aortic root sections from an *Apoe*$^{-/-}$ mouse stained for cell nuclei (DAPI, **blue**) and macrophages (CD68, **red)**, and autoradiography of an adjacent section after ^{89}Zr-LA25 injection; **below**: same aortic root section stained for endothelial cells (CD31, **green**), a merged image **(middle)**, and a 40× magnification **(right)**.

(F) Atherosclerotic mouse livers stained with LA24, LA25 (including 40× magnification), and no-antibody control section are shown. *$p < 0.05$.

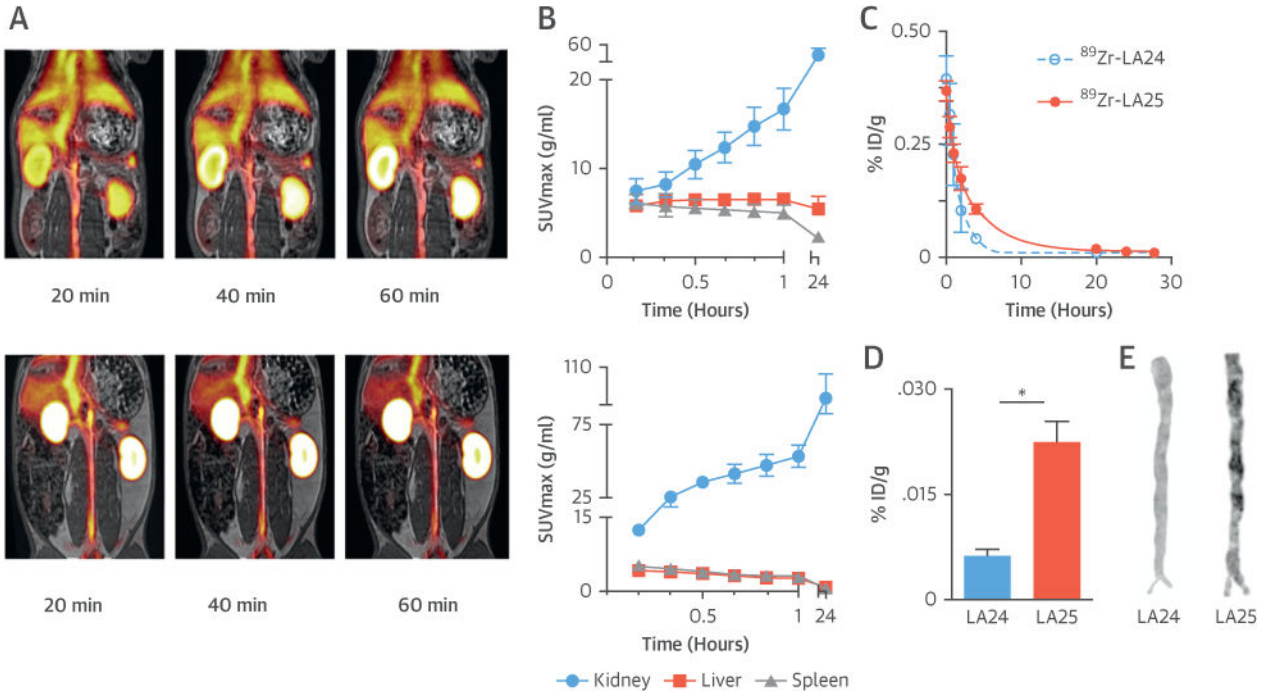

FIGURE 5. ^{89}Zr-LA25 PET/MR Imaging in Rabbits

(A) Representative coronal fused positron emission tomography (PET)/magnetic resonance (MR) images at 20, 40, and 60 min post-injection (p.i.) of ^{89}Zr-LA25 **(top)** and ^{89}Zr-LA24 **(bottom)**. **(B)** Radioactivity quantification in major organs in atherosclerotic rabbits based on PET/MR imaging (10 to 60 min), and 24 h p.i. **(C)** Pharmacokinetics in atherosclerotic rabbits for ^{89}Zr-LA24 and -LA25, with half-lives of 1.1 and 2.2 h, respectively. Ex vivo radioactivity concentration **(D)** and autoradiography **(E)** for ^{89}Zr-LA24 and -LA25 in aortas from rabbits with atherosclerosis 28 h p.i. *$p < 0.05$. SUV = standardized uptake value.

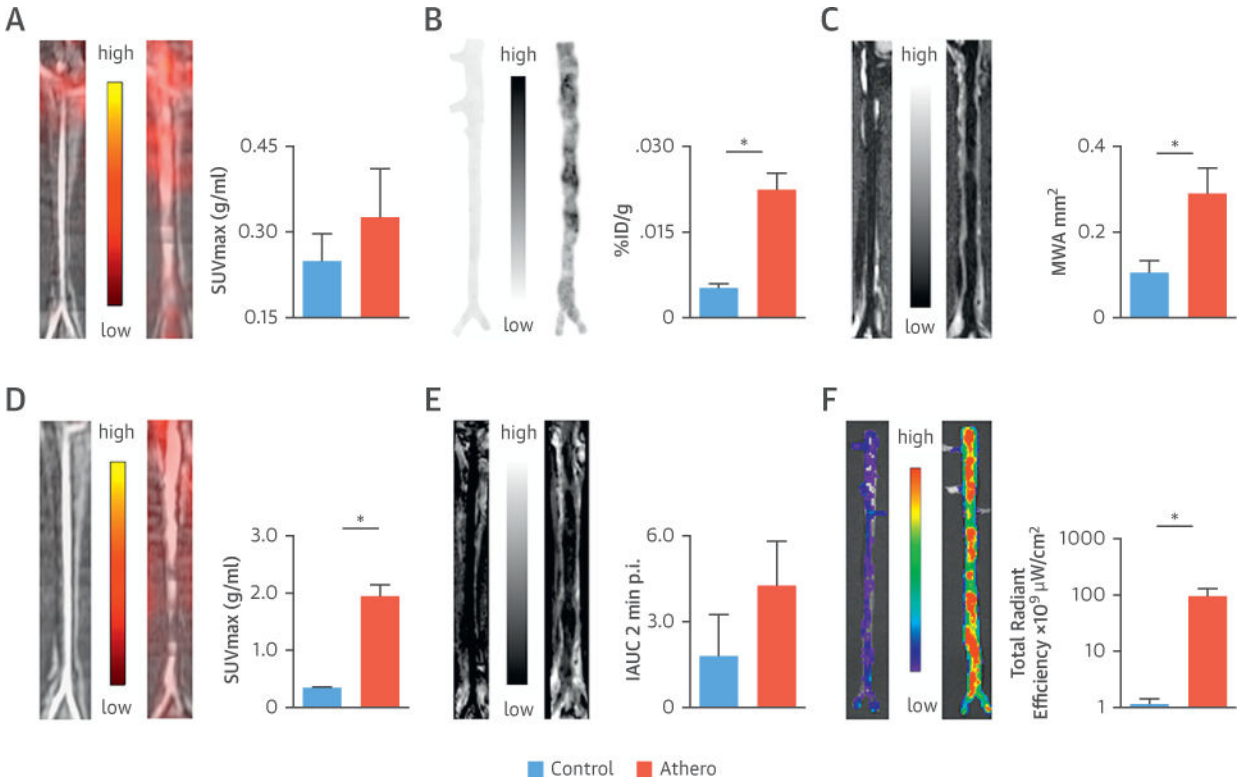

FIGURE 6. Phenotyping of Rabbit Atherosclerotic Plaques by PET/MR Imaging

(A) Representative coronal aortic fused PET/MR imaging 24 h p.i. of ^{89}Zr-LA25, **(B)** autoradiographs and gamma counting (whole aortas) 28 h p.i. of ^{89}Zr-LA25, **(C)** MR T2-weighted imaging, **(D)** ^{18}F-fluorodeoxyglucose (^{18}F-FDG) PET/MR imaging, **(E)** dynamic contrast enhanced (DCE)-MR imaging, and **(F)** fluorescently labeled (DiD)-rHDL near infrared fluorescence imaging, of healthy control **(white)** and atherosclerotic abdominal aortas **(black)**. *$p < 0.05$. IAUC = area under the normalized signal intensity curve; MWA = mean wall area; SUV = standardized uptake value.

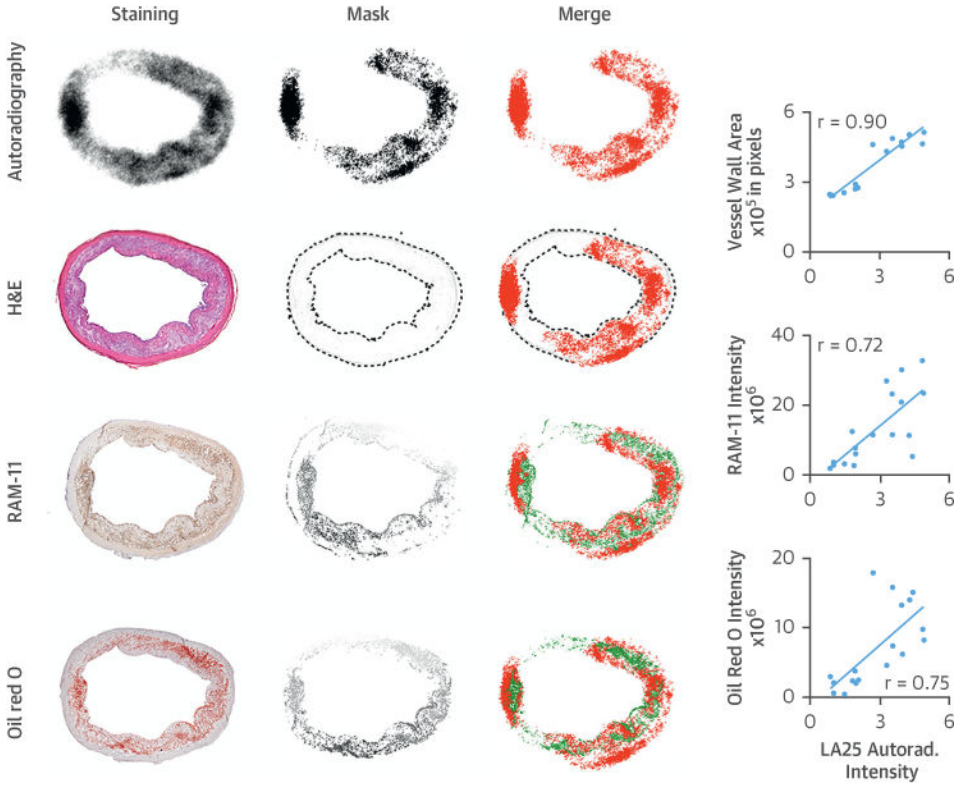

FIGURE 7. Ex Vivo Plaque Characterization

Digital autoradiography of atherosclerotic rabbit aorta sections with adjacent slides stained for hematoxylin and eosin, RAM-11, and Oil Red O, with corresponding masks and merged images with autoradiography. On the **right**, correlations are shown between autoradiography and vessel wall area, RAM-11, and Oil Red O.

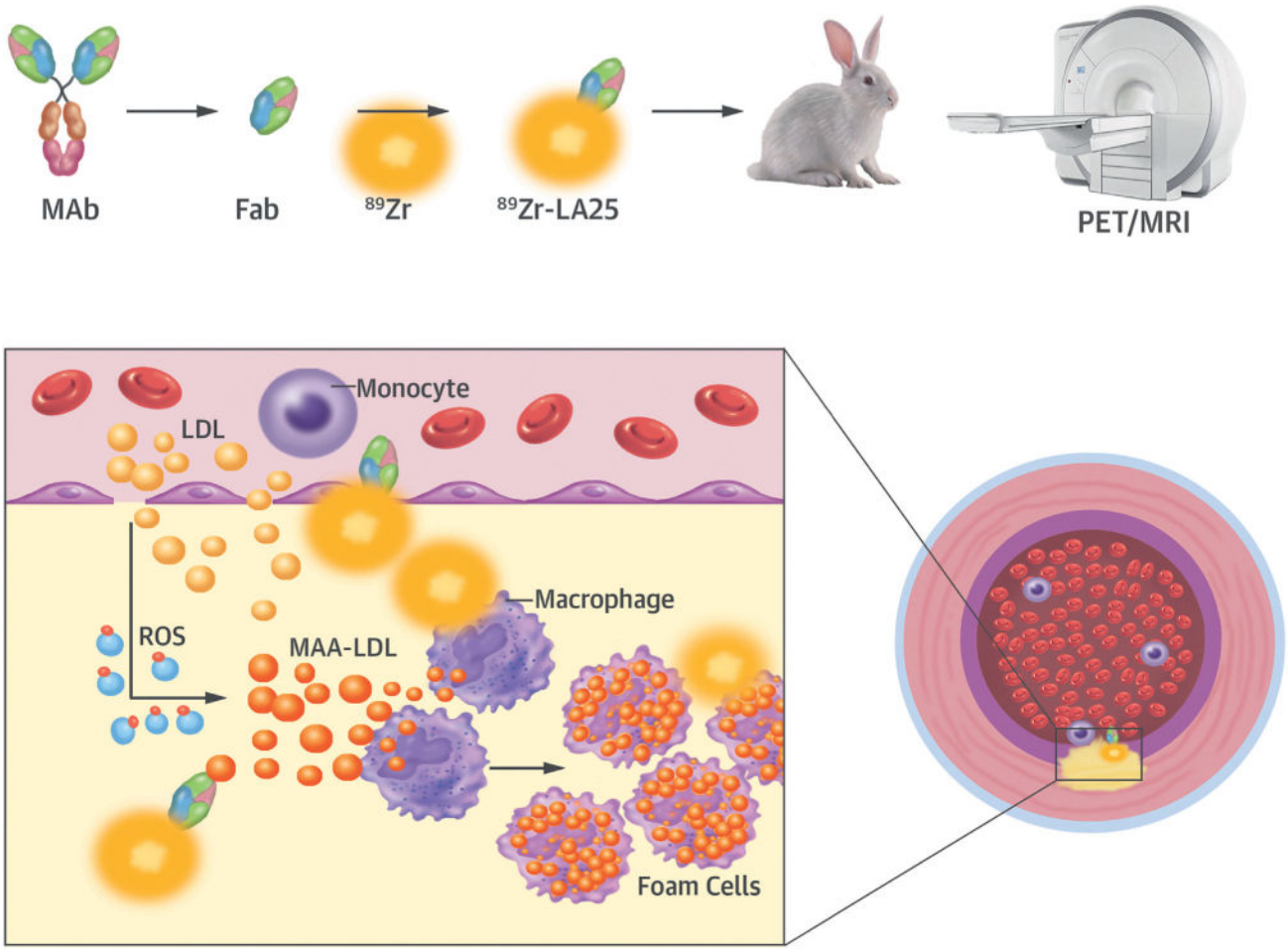

CENTRAL ILLUSTRATION. Targeting Atherothrombosis With ^{89}Zr-LA25

Atherosclerotic lesions are initiated by accumulation of lipoproteins. The modification of lipoproteins generates pro-inflammatory oxidation-specific epitopes, such as malondialdehyde-acetaldehyde (MAA) adducts, which lead to immune cell recruitment to the subintimal space. Accumulation of oxidized lipids results in foam cell formation and, ultimately, complex atherothrombotic lesions. LA25 is a human Fab antibody fragment discovered in the deoxyribonucleic acid (rather than plasma) of newborn babies prior to environmental exposure, consistent with evolutionary conservation. LA25 was found to specifically bind MAA epitopes and engineered to carry the positron emission tomography (PET) isotope ^{89}Zr. Using an integrated PET/magnetic resonance imaging (MRI) system, ^{89}Zr-LA25 was shown to noninvasively image mouse and rabbit atherosclerotic lesions, as well as MAA-rich steatotic livers. Fab = antigen-binding fragment; LDL = low-density lipoprotein; MAb = monclonal antibody; ROS = reactive oxygen species.